ORIGINAL ARTICLE

Carbon textile reinforced concrete: materials and structural analysis

Rebecca Mansur de Castro Silva · Flávio de Andrade Silva

Abstract Textile reinforced concrete (TRC) is a composite made of a cementitious matrix and non-corrosive fabrics with excellent mechanical behavior and elevated load-bearing capacity. Therefore, TRC is highly recommended for structural applications. Due to the reinforcement's non-corrosive property, this material is interesting in replacing the reinforced concrete (RC). This work presents a study on the characterization of carbon TRCs under tensile and bending loadings. Direct tensile tests were performed and the effect of the polymeric coating used on the fabric manufacturing, the number of layers and an epoxy resin and sand coating was analyzed. The results showed that the composites mechanical behavior depends mainly on the reinforcement-matrix bond. In order to evaluate the fabric-matrix interface, pull-out tests were carried on. The TRC potential as a structural application is also addressed. Thus, structural beams reinforced with carbon TRC with and without dispersed steel fibers on the matrix were submitted to bending. Compared with RC, the TRC beams presented less ductile behavior. Nevertheless, the current standards for the concrete structures design establish a maximum element displacement of span/ 250. At this level, the load–displacement curves of TRC and RC beams were coincident, and the applied load was considerably distant from the failure load.

Keywords Carbon textile reinforced concrete ·
Direct tensile tests · Pull-out tests · TRC structural
application

1 Introduction

Textile reinforced concrete (TRC) is a relative new cementitious matrix composite reinforced with one or multiple layers of 2D or 3D fabrics [1] that can be made of several types of fibers. Previous studies had shown the mechanical capacity of the TRC with AR-glass [2–4], basalt [5, 6], natural [7–10], and carbon [11–13] fabrics under direct tensile loading and bending. As shown, this material presents excellent mechanical behavior aligned with an elevated load-bearing capacity [14], and therefore it has been used for strengthening of existing concrete and masonry structures [15–26], and for the construction of new structural elements, such as slabs [27–29], self-supporting sandwich elements [30–35], and shell structures [36–39].

Reinforced concrete (RC) elements are prone to suffer corrosion. This degradation process can be accelerated by warm marine environments, in case of

R. Mansur de Castro Silva · F. de Andrade Silva (✉)
Department of Civil and Environmental Engineering,
Pontifícia Universidade Católica do Rio de Janeiro (PUC-Rio), Rua Marquês de São Vicente 225, Rio de Janeiro,
Rio de Janeiro 22451-900, Brazil
e-mail: fsilva@puc-rio.br

places near the coast, or deicing salts, used for deicing mostly highways and bridges in places that face severe winters [40]. The corrosion process can cause a reduction in the section of the steel reinforcement bar, and consequent loss of its tensile strength, and also a decrease in the bond between the concrete and the steel bar, which can lead to cracking and/or spalling of the concrete cover. These two mechanisms can cause loss of mechanical capacity of the RC member [41–44]. To guarantee safety and serviceability, considerable resources have to be expended in order to repair and rehabilitate deteriorate RC structures. Since the textiles are not prone to suffer corrosion, TRC becomes an interesting material to replace the RC in structural elements that are subjected to corrosion agents during their service life.

Carbon textiles are becoming extremely attractive as reinforcement for cementitious matrices due to the elevated mechanical and durability properties of the carbon fibers [45–48]. Previous studies [11, 49] show the elevated mechanical behavior of the carbon TRC under tensile and bending loadings. The main disadvantage of the carbon fabrics is their low bond with the cementitious matrix, which results in low composite mechanical performance. However, there are methods to improve the interaction between the fabric and the cementitious matrix, thus enhancing the mechanical behavior of the carbon TRC. One method to improve the bond between multifilament carbon yarns and cementitious matrices is the impregnation of mineral fillers. These particles size have to be sufficient to penetrate inside the bundle spaces and be able to produce a pozzolanic reaction with the cement matrix [12]. Peled et al. [50] showed that the silica fume with micro size particles provides an enhancement in the bond between the carbon yarn and the cementitious matrix, while the coating with nano silica filler drastically reduced the bond strength. This type of coating also presents a benefit in situations with high temperature and fire [51]. Organic coatings can also be used to improve the mechanical properties of carbon TRCs. Differently from the mineral fillers, the organic coating fills the spaces and binds all filaments within a yarn, forming a single unit. Thus, the load is efficiently carried by all filaments [52]. Donnini et al. [53] showed that a polymeric coating made of a flexible epoxy resin was able to improve the composite mechanical capacity, indicating an improvement on the bond between the carbon fabric and the cementitious matrix. The use of a sand layer over the resin was able to further increase the composite mechanical characteristics. Dvorkin and Peled [12] also showed an improvement of the composite mechanical properties when coating the carbon fabric with epoxy resin. Nevertheless marked delamination of the composite reinforced with carbon fabric coated with epoxy resin was observed during the tests. Xu et al. [54] also observed an improvement in the mechanical performance of TRCs with carbon fabrics coated with an epoxy resin. Another method to improve the bond between the carbon fabric and the cementitious matrix is prestressing the reinforcement during the composite manufacturing. The prestressing increases the friction between the inner filaments due to the Poisson's ratio effect and the bundling effect, which enhances the frictional bond strength and stiffness of the composite [54].

To evaluate the potential of the TRC in structural applications, Schummann et al. [27] conducted a large scale test in a parking slab made of carbon TRC with a new end anchorage method. Also, analytical calculations showed that the slab can be designed using the same principles from RC. May et al. [28] developed and investigated an element with a variable cross-section designed accordingly to the stress trajectory made of carbon TRC. Compared with a standard RC element with full cross-section a reduction of at least 50% of the structural self-weight could be achieved. The ultimate loads obtained for the carbon TRC element was higher than the calculated ultimate load for the common RC element. Moreover, applying a superelevation during the casting was possible to fulfill the limit values of the service limit state (SLC) established by Eurocode 2. Hegger et al. [32] demonstrated the successful application of an AR-glass TRC cladding panel as an exterior façade of an extension building in a pilot project at the Institute for Structural Concrete, in the Technical University of Aachen. The applicability of a carbon TRC shell structure was also demonstrated by Hegger et al. [39]. The building concept developed consisted of double curved, triangular load-bearing shell elements that could be mounted and disassembled as often as required. Scholzen et al. [36, 37] described the structural design and the construction method of a pavilion with a roof structure made of carbon TRC shells on the campus of RWTH Aachen University.

This work presents a study on the mechanical response of a carbon TRC submitted to direct tensile and bending loadings. Direct tensile tests were performed on composites reinforced with two types of carbon fabrics, each one with a different polymeric coating used during its manufacturing. The influence of the number of reinforcement layers and an additional epoxy resin and sand coating on the mechanical performance of the TRC was also evaluated. In order to evaluate the difference in the two types of carbon fabric-matrix interfaces, pull-out tests were carried on. Moreover, the potential of the carbon TRC as a structural application is presented. For this, structural beams made of carbon TRC with two layer of reinforcement on the longitudinal direction were submitted to four-point bending tests. The influence of dispersed steel fibers on the structural concrete element behavior and a textile reinforcement in the transversal direction was evaluated. The mechanical response of the carbon TRC beams was compared to steel reinforced concrete beams.

2 Experimental program

2.1 Materials

A cementitious matrix was used for both the characterization of the mechanical and bond behavior of the carbon textile reinforced concrete under direct tensile loading and the carbon textile reinforced concrete beams under bending. For the direct tensile and pull-out tests, the matrix was a fine-grained concrete with water/cementitious materials ratio of 0.3 constituted by Portland cement CPII F-32, defined by Brazilian standard [55], river sand with a maximum diameter of 1.18 mm, fly ash and silica fume. The average compressive strength was of 70 MPa and elastic modulus of 35 GPa, at 28 days. Meanwhile, a self-compacting concrete with (SCC-SF) and without (SCC) dispersed hooked end steel fibers was used as a matrix for the structural beams. The SCC had a water/cementitious materials ratio of 0.25 and was constituted by Portland cement CP-V ARI, defined by Brazilian standard [56], gravel with a maximum diameter of 9.5 mm, river sand with a maximum diameter of 0.850 and 0.150 mm, fly ash, silica fume and silica 325. The average compressive strength was 76 and 81 MPa and the elastic modulus was 40 and 35

GPa for the SCC and the SCC-SF, respectively. Table 1 shows the composition for the cementitious matrix and the self-compacting concrete.

As primary reinforcement, two types of bidirectional carbon fabrics were used—one with a styrene-butadiene resin (SBR) as polymeric coating, supplied by V. Fraas GmbH, and one with an epoxy resin (EPX) coating, developed by Solidian GmbH. Figure 1 shows the mesh opening of both carbon fabrics. From the inside to the inside of the yarn, the opening mesh is 10×8.5 mm and 11.5×10.5 mm for the SBR and EPX carbon fabrics, respectively. The yarn cross-sectional area was obtained through image analysis acquired on a stereoscopic microscope Nikon model SMZ800N with the software ImageJ. The cross-sectional areas obtained for warp and weft yarns, respectively, were 3.34 ± 0.12 and 3.30 ± 0.33 mm^2 for the SBR carbon fabric, and 5.44 ± 1.03 and 3.85 ± 0.24 mm^2 for the EPX carbon fabric. The tensile strength corresponds to 1700 MPa and 2700 MPa and the modulus of elasticity is 250 GPa and 220 GPa for the SBR and EPX carbon fabrics, respectively, according to the suppliers.

An additional coating made with epoxy resin Sikadur®-32 and sand was applied to the fabrics. The resin was placed with a sponge over both sides of the fabrics, and then sand was manually spread over the fresh resin. This process was performed 24 h before the composite manufacturing to guarantee that the resin was fully dry during casting. In this work, the textile reinforcement with this extra coating is referred to as coated fabric, whereas the textile reinforcement with only the polymeric coating used in its fabrication is referred to as plain fabric.

The steel fibers used as secondary reinforcement of the self-compacting concrete consisted of hooked ended fibers provided by Dramix® with 30 mm length, aspect ratio of 45, and tensile strength of 1270 MPa.

2.2 Composite manufacturing

For the direct tensile tests, the specimens consisted of rectangular plates measuring 1000 mm x 120 mm (length x width), that were produced using a lamination technique, as described in [57]. A thin layer of the matrix was placed in a steel mold, and the first layer of the fabric was positioned over the fresh matrix, then another thin layer of matrix was placed over it. This procedure was repeated until that the desired number

Table 1 Cementitious matrices composition

Composition (kg/m^3)	Fine-grained concrete	SCC	SCC-SF
Cement Type CPII F-32	632	–	–
Cement Type CP-V ARI	–	360	360
Gravel (9.5 mm)	–	492	438
River sand (0.850 mm)	–	100	100
River sand (0.150 mm)	947	827	827
Fly ash	265	168	168
Silica fume	50.5	45	45
Silica 325	–	70	70
Water	279.7	166	166
Superplasticizer	6.31	19,8	19,8
Steel fiber	–	–	157

(a)   **(b)**
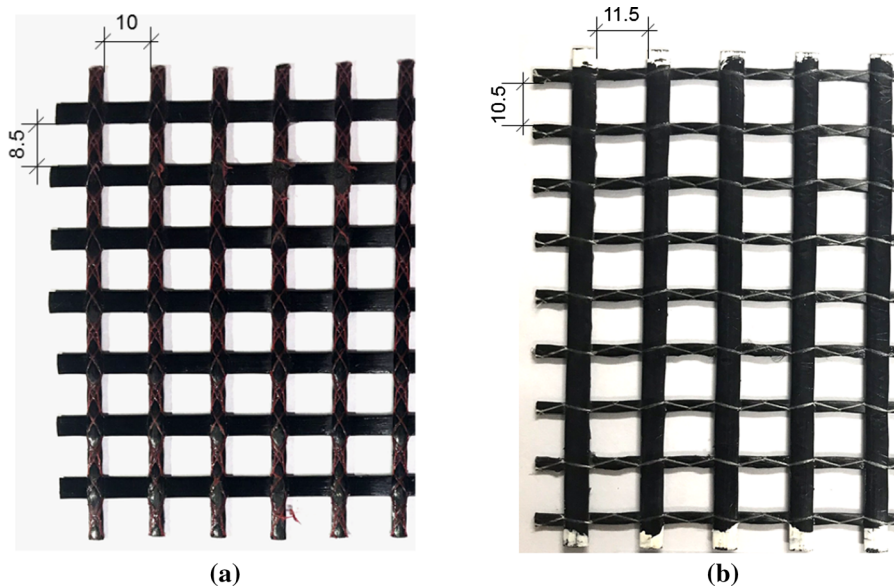
Fig. 1 Opening mesh of the (**a**) SBR and (**b**) EPX carbon fabrics (Dimensions in mm)

of reinforcement layers was achieved. In order to reduce the cross-sectional area in the mid-span, and therefore facilitate the specimen failure in that region during the test, two aluminum plates were used. The plates had 500 mm × 120 mm × 1.5 mm (length × width × thickness) and one of them was set at the bottom of the mold, before the first layer of matrix was placed, and the other at the top of the specimen. This technique was not used for the TRC with one and two layers of the plain SBR carbon fabric since they were the first specimens to be tested. From the experience gained from these tests, the authors decided to improve composite manufacturing to obtain better tensile test results. Therefore, the specimens referred

to as 1SBR and 2SBR (see Table 2) presented a uniform thickness through their entire length. The thickness of the specimens, indicated in Table 2, varied according to the type of the fabric, the presence or not of the extra epoxy resin and sand coating, and the number of fabric layers. For the specimens with reduced cross-sectional area in the mid-span, the thickness presented in the table refers to this thinner region. At least four specimens were tested for each type of composite, and the thickness presented corresponds to the average value. The specimens were wetted, involved in a plastic film and stored in a room with controlled temperature (20 ± 2 °C) and humidity (55 ± 5%) for 28 days.

The specimens for the pull-out tests were prepared according to [57]. They consisted of small cylinders that were cast in PVC molds with 25×20 mm (diameter $\times$ height) supported on an acrylic plate. The fine-grained concrete was placed in the molds and one yarn of the SBR and EPX carbon fabrics, with and without the extra coating of epoxy resin and sand, was positioned in the center of the cylinders. The embedded length of the yarns was 20 mm. The specimens were removed from the molds after 24 h and stored in a wet chamber with 100% of humidity and temperature of 21 ± 2 °C for 7 days. At least eight specimens of each type of composite were tested.

For the structural tests, five carbon textile reinforced concrete beams were produced, varying the type and direction of the textile reinforcement and the volume fraction of short steel fibers added in the concrete matrix, according to Table 3. The longitudinal and transversal directions are related to the beam axis. The beams had $1200 \times 150 \times 150$ mm (length $\times$ width $\times$ height) with a 25 mm notch in the mid-span section and two layers of textile reinforcement with the extra coating of epoxy resin and sand in the longitudinal direction. The number of longitudinal reinforcement layers was determined to obtain flexural load capacity similar to that of conventional steel reinforced concrete beams so that their mechanical behaviors could be compared (see Sect. 3.3). Two design methodologies were used, one based on the flexural design of TRC elements of the Rilem Report 36 [14], and the other based on the Brazilian Code NBR 6118:2014 [58], in which an approximation was made, and the carbon textile reinforcement was considered in place of the longitudinal bar steel. Both results presented similar textile reinforcement ratios, corresponding to approximately 2 layers of both SBR and EPX carbon fabrics. The longitudinal textile reinforcement ratio was 0.352% and 0.435% for the SBR and EPX carbon fabrics, respectively. The longitudinal textile reinforcement ratio is the proportion of the cross-sectional area of the textile reinforcement in the longitudinal direction to the cross-sectional of the element and it is shown in Table 3. The specimens with only longitudinal textile reinforcement were cast using a hand lay-up technique: (1) a thin layer of concrete was placed in a wood mold, (2) the first fabric layer was positioned over it, (3) another thin layer of concrete was placed over the fabric, (4) the second and last layer of fabric was positioned over

it, (5) the concrete was placed in the mold up to the top of it. The beam with both longitudinal and transversal textile reinforcement was cast similar to a conventional steel reinforced concrete beam; first, the reinforcement (Fig. 2) was positioned in the mold and then the concrete was poured over it and then compacted. All five beams were air cured for 28 days.

2.3 Testing procedures

2.3.1 Direct tensile tests

To evaluate the mechanical behavior of the carbon textile reinforced concrete direct tensile tests were performed. The tests were conducted in an MTS 311 universal testing machine with a capacity of 1000 kN and controlled by the actuator displacement at a rate of 0.5 mm/min. The load cell of the MTS system is calibrated at different load levels. In this research, it was used the load level from 0 to 100 kN. The specimens were tested using a gage length of 500 mm, and to achieve their displacement, two linear variable differential transducers (LVDTs) were used. Since, their reading capacity was of 250 mm, inferior to the gage length; an extensor made of aluminum was attached to their extremities. The ends of the specimens were connected to steel plates with screws (Fig. 3). Torque was applied to these screws in order to avoid slippage between the specimens and the steel plates. Also, emery papers were glued at the surfaces of the specimens that were in contact with the steel plates. To guarantee the complete failure of the specimens, and consequently obtain the tensile strength of the material, the boundary conditions (number of screws, torque and contact surface between the specimen and the steel plate) were varied according to the type of composite (Table 2).

The tensile stress was calculated dividing the load recorded from the machine load cell by the composite area (width x thickness of the gage length). The strain was obtained by the division of the average displacement measured by the LVDTs and the gage length of the specimen.

2.3.2 Pull-out tests

In order to study the difference in the bond behavior of the textile reinforced concrete with SBR and EPX carbon fabrics, pull-out tests were performed. An MTS

Table 2 Properties of the composites tested under direct tensile loading

Specimen	1SBR	2SBR	1SBR-S	2SBR-S	1EPX	2EPX	1EPX-S	2EPX-S
Type of carbon fabric	Plain SBR	Plain SBR	Coated SBR	Coated SBR	Plain EPX	Plain EPX	Coated EPX	Coated EPX
Number of Layers	1	2	1	2	1	2	1	2
Thickness (mm)	10.2 (0.879)	12.3 (0.898)	9.23 (0.400)	11.4 (0.742)	6.39 (0.334)	9.09 (0.309)	7.98 (0.251)	11.4 (0.541)
Boundary conditions								
Number of screws	8	8	8	10	10	12	10	10
Torque (Nm)	18	18	19	25	18	34	29	44
Contact surface (mm^2)	18,000	18,000	24,000	24,000	24,000	24,000	24,000	24,000
Direct tensile results								
σ_{max} (MPa)	6.49 (0.664)	8.34 (0.619)	19.1 (2.59)	32.8 (4.82)	41.3 (8.00)	33.8 (5.33)	52.4 (3.73)	51.6 (5.17)
$\varepsilon_{\sigma,max}$ (mm/mm)	0.0120 (0.00169)	0.0130 (0.00114)	0.00554 (0.00100)	0.00773 (0.00216)	0.00810 (0.00101)	0.00511 (0.000751)	0.0122 (0.00145)	0.0118 (0.00135)
σ_{BOP} (MPa)	2.59 (0.562)	3.66 (0.611)	2.53 (0.463)	2.54 (0.340)	2.59 (0.142)	3.15 (0.460)	2.60 (0.548)	2.98 (0.491)
ε_{BOP} ($\times 10^{-3}$ mm/mm)	0.151 (0.0854)	0.179 (0.0628)	0.265 (0.0547)	0.115 (0.0448)	0.185 (0.0226)	0.176 (0.0472)	0.243 (0.0665)	0.185 (0.0993)

universal machine model 810 with a capacity of 250 kN was used to carry on the tests. Due to the low load values, a load cell with 2.5 kN capacity was coupled for obtaining more accurate results. The specimens were fixed at their bottom inside a metal cup and the yarn was pulled-out, at a displacement rate of 1.5 mm/min, by a metal claw that was connected to the machine, as shown in Fig. 4. The metal claw was positioned as close as possible of the top surface of the matrix. The yarns slip was obtained directly from the machine displacement.

The average interfacial shear stress (τ) was obtained through the equation below:

$$\tau = \frac{P_{max}}{2\pi r l} \tag{1}$$

where P_{max} is the maximum pull-out load, l is the embedded length (20 mm) and r is the equivalent radius of the yarn, assuming a circular yarn.

2.3.3 Bending tests

To evaluate the structural capacity of the carbon textile reinforced concrete, four-point bending tests were performed in an MTS servo-controlled hydraulic system with 500 kN capacity. The tests were controlled by displacement at a rate of 1 mm/min and two LVDTs were used to obtain the mid-span deflection of the beams. As shown in Fig. 5, the beams were positioned over support rollers separated by a span of 1100 mm. The load was applied by rollers spaced by 370 mm from each other, and each individual roller was distant 185 mm from the mid-span section of the beam. Both support and load application rollers had free horizontal displacement.

3 Results and discussion

3.1 Direct tensile tests

The tensile stress–strain curves obtained can be characterized by three distinct stages, as shown in Fig. 6. Stage I corresponds to the elastic-linear region, where the matrix and the textile reinforcement behave linearly. The bend over point (BOP) is the point where occurs the first matrix crack, and it divides Stages I and II. After the matrix is cracked, the TRC does not present a reduction in its load-carrying capacity

Table 3 Characteristics of the carbon TRC beams

Specimen	SBR-L0%	EPX-L0%	SBR-L2%	EPX-L2%	SBR-LT2%
Type of carbon fabric	Coated SBR	Coated EPX	Coated SBR	Coated EPX	Coated SBR
Textile reinforcement direction	Longitudinal	Longitudinal	Longitudinal	Longitudinal	Longitudinal and Transversal
Longitudinal textile reinforcement ratio	0.352%	0.435%	0.352%	0.435%	0.352%
Steel fiber V_f	0%	0%	2%	2%	2%
Experimental					
P_{max} (kN)	34.2	38.7	79.4	72.2	94.0
$\delta_{P,max}$ (mm)	11.6	12.9	12.2	17.7	15.5
$M_{max,exp}$ (kNm)	6.3	7.1	14.6	13.2	17.2
P_{LOP} (kN)	12.0	16.8	26.5	30.7	21.2
δ_{LOP} (mm)	0.676	0.768	0.910	1.05	0.596
Failure mode	Shear	Shear	Shear and flexure	Shear	Flexure
Theoretical (Rilem report 36)					
$M_{max,theo}$ (kNm)	12.4	18.3	12.4	18.3	12.4
$\frac{M_{max,exp}}{M_{max,theo}}$	0.51	0.39	1.18	0.72	1.39
Theoretical (Henager and Doherty's Model)					
$M_{max,theo}$ (kNm)	17.6	32.6	18.8	33.8	18.8
$\frac{M_{max,exp}}{M_{max,theo}}$	0.36	0.22	0.78	0.39	0.91

because the textile reinforcement offers ways to transfer the stresses through the cracks. Stage II is characterized by a multiple crack formation as the applied strain increases. In Stage III there is no opening of new cracks, only the widening of the existing ones. Thus, the increasing strain of the composite is majorly due to the stretching of the fabric. This strain hardening behavior is not trivial to be achieved with the opening mesh of the carbon fabric used as reinforcement [59], which indicates that the specimen geometry and the boundary conditions used for the direct tensile tests are efficient.

Figure 6 shows the representative tensile-stress curves and Table 2 the average results and the standard deviation for the tensile strength (σ_{max}), the strain at tensile strength ($\varepsilon_{\sigma,max}$), the bend over point tensile stress (σ_{BOP}) and the bend over point strain (ε_{BOP}) obtained for all the specimens tested in direct tensile loadings. As Silva and Silva [57] previously described, the tensile mechanical performance of the TRC with EPX carbon fabric was superior to the one of the TRC with SBR carbon fabric. The tensile stress–strain curve of the TRC with SBR carbon fabric was flatter, not reaching high tensile stress values. The tensile strength of the EPX composites was approximately 630% and 400%, for one and two, layers respectively, higher than the tensile strength of the SBR. However, the TRC with SBR carbon fabrics presented higher pseudo-ductility. The strain at the tensile strength of the TRC with SBR carbon fabric was approximately 150% and 250%, for one and two layers, respectively, greater than for the TRC with EPX carbon fabric. This type of curve, flatter with low tensile stresses and elevated pseudo-ductility, is characteristic of TRC in which the textile reinforcement present low bond with the cementitious matrix [14]. Therefore, this could indicate that the bond between the SBR fabric and the cementitious matrix is not as strong as the bond between the EPX carbon fabric and the cementitious matrix. This difference may be related to the chemical affinity of the different polymeric coatings with the cementitious matrix, but also to differences regarding the mechanical and physical properties of the coatings. The epoxy resin
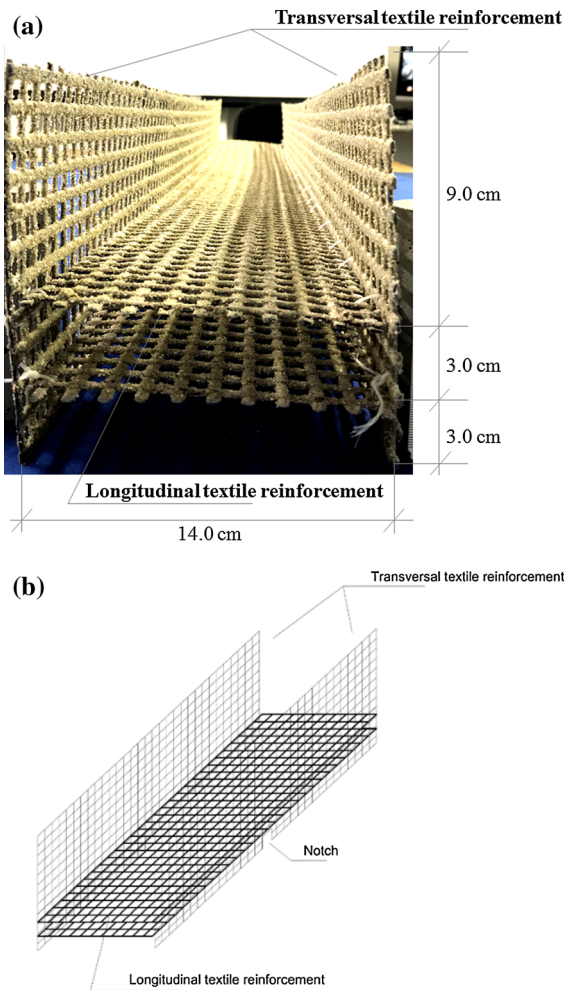
(a)

(b)

Fig. 2 Reinforcement layout for the FLT2% beam. **a** Transversal view and **b** schematic textile reinforcement configuration

Fig. 3 Direct tensile test setup

seems to present more chemical affinity with the cementitious matrix than the SBR. Moreover, the rheology of the polymeric coating can also influence in its ability to fill the spaces inside the yarn, guaranteeing that all filaments have a bond with the matrix [11, 14, 53]. Further analysis should be carried on to better understand the mechanisms involved in textile reinforcement-matrix bond.

The addition of the epoxy resin and sand coating improved the tensile strength of the TRC with both carbon fabrics. This improvement was approximately of 200% and 300% for the TRC with SBR carbon fabric with one and two layers, respectively; and of 30% and 50% for the TRC with EPX carbon fabric with one and two layers, respectively. The

enhancement on the tensile strength was significantly more pronounced in the composites with the SBR carbon fabric. Furthermore, the addition of the epoxy resin and sand coating modified the tensile stress–strain curves of the TRC with SBR carbon fabric. They were able to reach higher tensile stresses, but with no pseudo-ductility. This could indicate an enhancement on the bond of the coated SBR carbon fabric and the cementitious matrix, which could be due to the mechanical bonding provided by the sand. Similar results were observed by Donnini et al. [53] and Yin et al. [60]. The TRC with coated EPX carbon fabrics also did not present pseudo-ductility.

The TRCs with two layers of plain and coated SBR carbon fabrics presented tensile strength approximately 30% and 70% higher than the TRC with only one layer. This enhancement was expected due to the increase in the reinforcement volume fraction. The reinforcement volumetric fraction of the composites reinforced with the SBR carbon fabric is 2.44% and 4.05% for 1 and 2 reinforcement layers, respectively. Thus, there was an increase of approximately 65% in the reinforcement volume fraction. The reinforcement
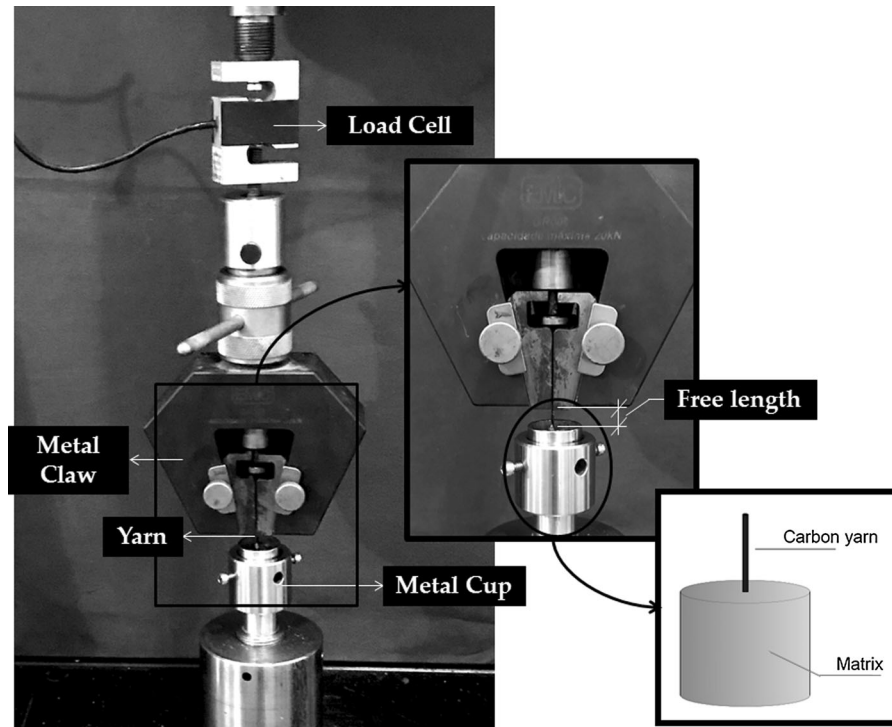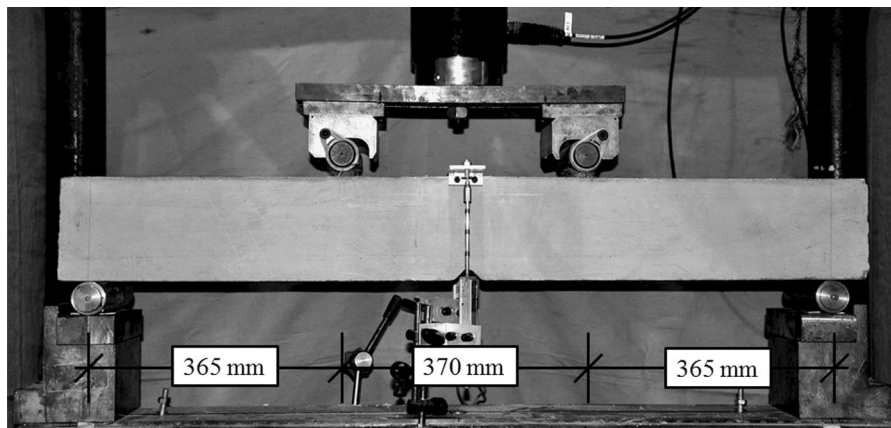
Fig. 4 Pull-out test setup

Fig. 5 Four-point bending test setup

volume fraction is a ratio of the reinforcement amount to the matrix amount in a composite. The thickness and, consequently, the cross-sectional area of these composites was approximately the same (see Table 2). Thus, with the increase in the number of textile layers, there is an enhancement of the reinforcement volume fraction. According to the rule of mixture, the upper limit composite properties are the weighted average of the properties of its components [47]. Another reason for the stress hardening being more pronounced in the composites reinforced with two layers could be related to the less or retarded cracking of the matrix portion in between the layers. Therefore, its contribution to the total axial load may be higher compared to the matrix
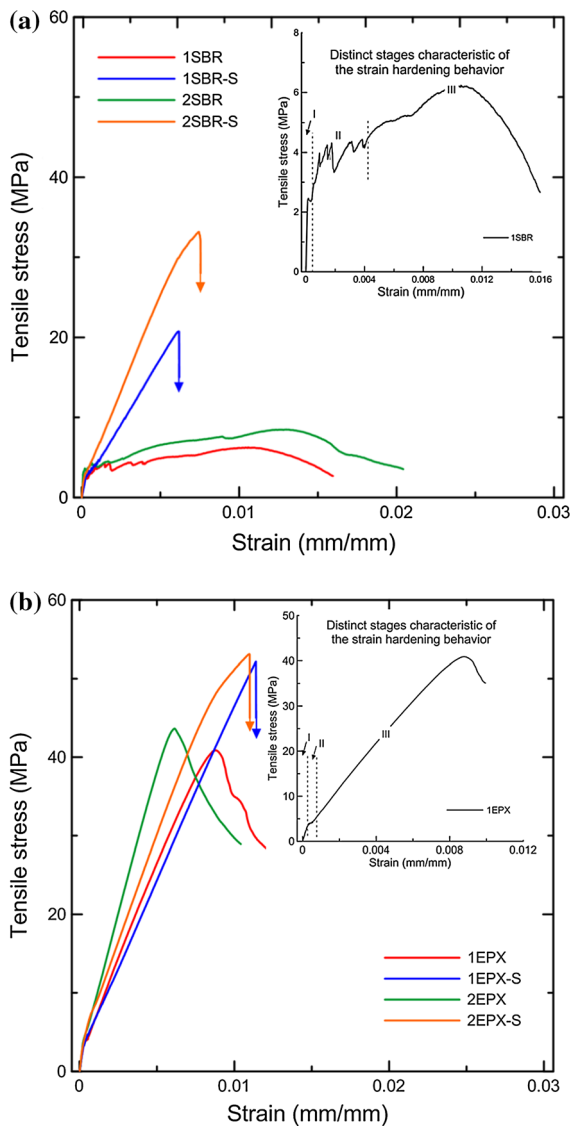
Fig. 6 Representative tensile stress-strain curves obtained from the direct tensile tests for the **a** SBR carbon TRCs and **b** EPX carbon TRCs

in the external portions. The central portion receives bonding actions from the fabric layers on both sides. For the specimens with the EPX carbon fabric, the number of layers did not affect significantly the tensile strength. Taking into account the standard deviation, the tensile strength of composites with one and two layers of plain and coated EPX carbon fabric was approximately the same. The reinforcement volumetric fraction of these composites is 4.52% and 6.35% for 1 and 2 reinforcement layers, respectively,

indicating an enhancement of approximately 40%. Although there was an increase in the reinforcement volume fraction, it was less pronounced than the one for the composites reinforced with the SBR carbon fabric. Furthermore, it is important to note that the reinforcement volumetric fractions were calculated using the cross-sectional areas of composites and fabrics, and in this case, only the longitudinal yarns are considered. However, since the fabrics are bi-directional, the transversal yarns can significantly affect the value of the volumetric fraction.

The results obtained are in accordance with those available in the literature [11, 12, 53, 61, 62]. Dvorkin and Peled [12] obtained maximum tensile stress of about 60 MPa for a TRC with carbon fabric impregnated with an epoxy resin, which is in the same order of magnitude of the results acquired for the composites with the EPX carbon fabric. Holz et al. [62], considering the reinforcement area to calculate the tensile stress, found maximum stress of about 2000 MPa for a TRC with two layers of carbon fabric coated with SBR and epoxy resin and sand only in the load transference area. This value is compatible with the maximum stress obtained for the composite with one layer of the SBR fabric coated with epoxy resin and sand, which is about 1500 MPa, using the reinforcement area for calculation. Donnini et al. [53, 61], also using the reinforcement area, obtained maximum stress varying from 713 to 1366 MPa for a TRC with a carbon fabric coated with different levels of epoxy resin and sand. This result is consistent with the maximum stress obtained in this research for the composite with one layer of the EPX carbon fabric coated with epoxy resin and sand, which is about 1400 MPa, also using the reinforcement area for calculation.

3.2 Pull-out tests

Pull-out tests were performed to evaluate the difference in the bond of the SBR and EPX carbon yarns and the cementitious matrix. Figure 7 shows the representative pull-out load-slip curves obtained from the pull-out tests. Table 4 presents the average results and the standard deviation for the maximum pull-out load (P_{max}), the average interfacial shear stress (τ), and the slip at maximum pull-out load (δ_{max}) obtained from the pull-out tests.

The yarn from the plain EPX carbon fabric presented a higher maximum pull-out load than the

yarn from the plain SBR carbon fabric, which could indicate that the EPX carbon yarn presents a bond with the cementitious matrix superior to the SBR carbon yarn. The main differences between the two types of carbon fabrics are their tensile strengths and the polymeric coating used in their manufacturing. However, as the bond between the textile reinforcement and the cementitious matrix is the weakest region of the composite, the failure of the composite occurs before the fabric reaches its tensile strength. Thus, it is the bond that governs the behavior of the composite until its failure, and the difference in the tensile strengths does not play a major role. Therefore, these results confirm that the epoxy resin seems to be more efficient in enhancing the bond between the carbon fabric and the cementitious matrix than the SBR, supporting the better performance of the TRCs with the EPX fabric in the direct tensile tests.

The addition of an epoxy resin and sand coating enhanced the maximum pull-out load of the SBR yarn, indicating that there was an improvement in the reinforcement-matrix interface, which could be due to the mechanical bonding provided by the sand. Similar results were also found by Shilang and He [63] and Yin et al. [60]. The addition of this extra coating did not affect significantly the maximum interfacial shear stress of the EPX yarn since its bond with the cementitious matrix was already higher. The carbon TRC behavior under tensile loading is supported by the results of the pull-out tests.

3.3 Bending tests

The structural capacity of the carbon textile reinforced concrete was evaluated through four-point bending tests performed in structural beams. Figure 8 shows the load–displacement curves and Table 3 the results for the maximum applied load (P_{max}), the displacement at maximum applied load (δ_{max}), the load at the first matrix crack (P_{LOP}), the displacement at the first matrix crack (δ_{LOP}), and the failure mode obtained for the five beams tested.

The EPX-L0% beam presented more flexural macro-cracks (14 flexural macro-cracks) than the SBR-L0% beam (6 flexural macro-cracks). The flexural macro-cracks were visually accounted from photos taken during and after the tests. The flexural cracks of the SBR-L2%, EPX-L2%, and SBR-LT2% were too small to be observed and accounted. The

EPX-L0% and EPX-L2% beams presented superior stiffness than the SBR-L0% and SBR-L2% beams at low displacement levels. In the post-multiple-cracking stage, the SBR-L2% and SBR-LT2% beams presented similar stiffness. However, due to the reinforcement in the transversal direction, the SBR-LT2% beam supported higher applied loads.

The addition of dispersed steel fibers in the concrete matrix enhanced the first matrix crack load for the beams reinforced with both carbon fabrics. Hinzen e Brameshuber [64] had already confirmed this effect in tensile tests. Accordingly to Barhum and Mechtcherine [4] three mechanisms can be described to explain the enhancement of the first matrix crack load due to the addition of dispersed fibers in the concrete. The first mechanism is related to the matrix shrinkage. The dispersed fibers reduce the matrix shrinkage, and thus the concrete internal damage. Moreover, the dispersed fibers prevent the opening and consequently micro cracks coalescence caused by shrinkage and external load application, characterizing the second mechanism. Therefore, higher loads are necessary so that the first matrix crack occurs. The last mechanism is related to the reinforcement volume fraction. The addition of the dispersed fibers enhances the reinforcement volume fraction of the element and accordingly to the composites theory [47], if the bond between the reinforcement and the matrix is elevated, the first matrix crack is proportional to the reinforcement volume fraction. In the present study, the incorporation of the steel fibers enhanced the reinforcement volumetric fraction from 0.352% to 2.352% and 0.435% to 2.435% for the beams reinforced with the SBR and EPX carbon fabrics, respectively. Due to the good bond between the reinforcement and the cementitious matrix, the first matrix crack strength could be enhanced.

Moreover, the beams with dispersed steel fibers presented superior maximum applied load, due to the capacity of these fibers in helping in the absorption of tensile forces through the diagonal crack, and thus contribute to the bending. Previous studies [65–68] show that the addition of dispersed fibers in the concrete considerably enhances the shear strength of elements under flexure loading. In elements without stirrups, i.e., without conventional transversal reinforcement, these fibers can lead to multiple diagonal cracking, enhancing the element ductility.
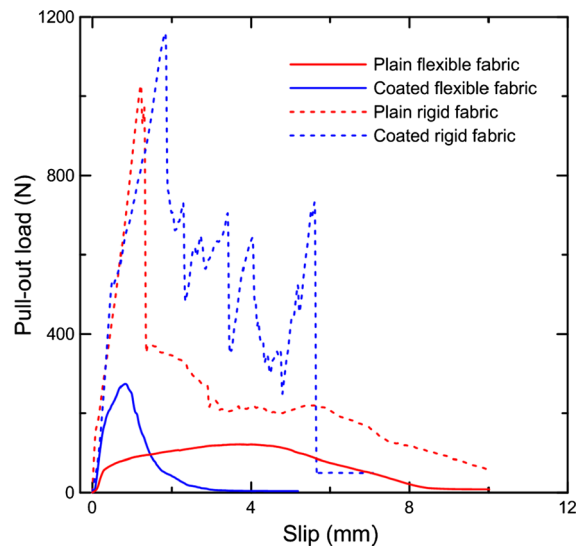
Fig. 7 Representative pull-out load-slip curves obtained from the pull-out tests

Table 4 Average results and standard deviation obtained from the pull-out tests

Specimen	P_{max} (N)	τ (MPa)	δ_{max} (mm)
Plain SBR yarn	91.2 (22.6)	0.705 (0.105)	2.63 (2.36)
Coated SBR yarn	232 (86.1)	1.57 (0.860)	1.01 (0.384)
Plain EPX yarn	987 (120)	4.17 (2.80)	1.57 (0.22)
Coated EPX yarn	894 (135)	5.39 (0.817)	1.91 (0.443)

The SBR-L0% and EPX-L0% beams presented a shear failure, which was already expected since they did not have any type of reinforcement to support shear stresses. The EPX-L2% beam, even with the presence of the dispersed steel fibers also presented a shear failure. Figure 9a shows the failure mode of the SBR-L0% beam, exemplifying the shear failure. The SBR-L2% beam presented a failure by shear and flexure. As show in Fig. 9b, the crack that led to the failure of the SBR-L2% beam started in the direction of one of the load points application, where both the shear and the bending are maximum. Therefore, the volume fraction of dispersed steel fibers added was not able to prevent the shear failure of the beams. The SBR-L0%, EPX-L0%, SBR-L2%, and EPX-L2% beams also showed flexure cracks which followed a space pattern between them that are typical of TRCs, as can be seen in Fig. 9a. In the SBR-L2%, and EPX-L2% beams these cracks were so small that is not

possible to identify them in the pictures (Fig. 9b). In the detail of Fig. 9b, it is possible to observe the steel fibers bridging the cracks. The SBR-LT2% beam presented a flexure failure, indicating that the dispersed steel fibers and the carbon fabric in transversal direction were able to support the shear stresses.

For the beams with shear failure (Fig. 9a), the crack that led to the element rupture was diagonal, in the direction from the load application point to the support. The crack propagated diagonally until finding a textile layer, where it started to propagate horizontally. Hegger et al. [69] found this same failure mode for beams reinforced with AR-glass fabrics. These horizontal cracks along the longitudinal reinforcement are typical of the dowel action [70]. The shear strength of a steel reinforced concrete cracked section depends on four mechanisms: the transfer of the forces through the non-cracked zone, the transversal reinforcement capacity, the aggregate interlock, and the dowel action [71]. In elements without conventional transversal reinforcement, the shear stress is only transferred by the two last mechanisms, the aggregate interlock, and the dowel action. The dowel action can be defined as the capacity of the longitudinal reinforcement of transferring stresses perpendicular to its axis [70]. Due to the higher stiffness of the reinforcement to the matrix, the longitudinal reinforcement acts as a bridge, connecting the element sections between the matrix cracks. This effect increases the matrix region that contributes to the transmission of shear forces. According to El-Ariss [72], the dowel action importance is inversely proportional to the amount of transversal reinforcement. Therefore, the dowel effect plays an important role in the shear capacity of the SBR-L0%, EPX-L0%, SBR-L2%, and EPX-L2% beams, which did not present stirrups for shear reinforcement.

Theoretical values for the maximum bending moment of the TRC beams tested were obtained using the design model for textile reinforced concrete elements submitted to bending proposed by the Rilem Report 36 [14] and the simplified Henager and Doherty's model [73]. In the Rilem Report 36, the bending capacity of the TRC beams is obtained analogously to steel reinforced concrete. However, an additional factor needs to be taken into account due to the effect of beam curvature on the reinforcement. The maximum bending moment can be obtained from the following equations.
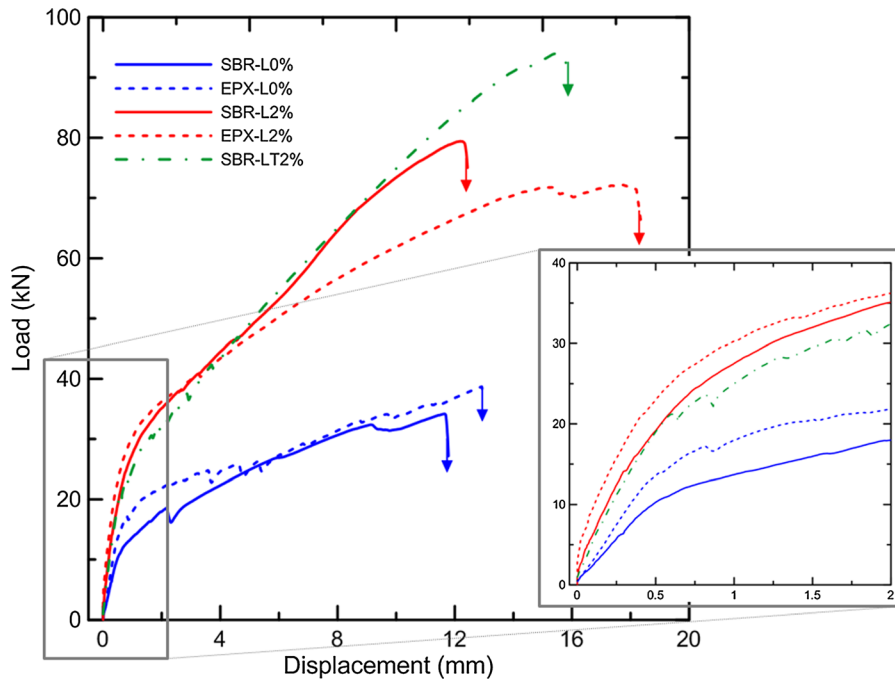
Fig. 8 Load-displacement curves obtained from the four-point bending tests

$$M_{\max} = k_{fl,p}.F_{\mathrm{ctu}}.z \tag{2}$$

$$F_{\mathrm{ctu}} = k_1.k_2.k_{0,\alpha}.A_t.f_t \tag{3}$$

$$k_1 = \frac{\sigma_{\max}}{f_t} \tag{4}$$

where $k_{fl,p}$ is the factor due to the beam curvature; F_{ctu} is the tensile strength of the reinforcement; z is the inner lever arm; k_1 is the factor for the textile efficiency; k_2 is the factor for biaxial loading; $k_{0,\alpha}$ is the factor for orientation of the reinforcement; A_t is the cross-sectional area of the reinforcement; f_t is the tensile strength of the reinforcement; and $\sigma_{\max}$ is the tensile strength of the reinforcement in the composite, obtained from the direct tensile tests using the reinforcement cross-sectional area. Usually $z \sim 0.9d$ and $d \sim 0.9h$, where d and h are the effective and full depth, respectively. In this research k_1 and k_2 were assumed 1.

For carbon fabrics,

$$k_{fl,p} = 0.9 + 0.55 \frac{A_t}{A_c} \tag{5}$$

where A_t and A_c are the cross-sectional areas of the

reinforcement and the element, respectively. Differently from the method proposed by the Rilem Report 36, the Henager and Doherty's model considers the effect of short fibers on the tensile strength of concrete. In this model, the bending strength of a steel reinforced concrete beam with dispersed fibers is determined by assuming rectangular blocks for the concreted in the tension and compression zones (Fig. 10). Considering the Henager and Doherty's model for a beam with longitudinal textile reinforcement and assuming $d \sim 0.9h$, the following non-dimensional parameters can be obtained from equilibrium conditions:

$$k_x = \frac{x}{h} = \frac{\rho_t {f_t}/{f_c} + {f_{\mathrm{ctr}}}/{f_c}}{{f_{\mathrm{ctr}}}/{f_c} + \eta\lambda} \tag{6}$$

$$\begin{aligned}
\mu &= \frac{M}{A_c h f_c} \\
&= \rho_t \frac{f_t}{f_c}\left(0.9 - \lambda\frac{k_x}{2}\right) + \frac{f_{\mathrm{ctr}}}{f_c}\frac{(1 - k_x)}{2}[1 - (1 - \lambda)k_x]
\end{aligned} \tag{7}$$

where M is the bending moment; f_c is the compressive strength of concrete; f_{ctr} is the residual tensile strength
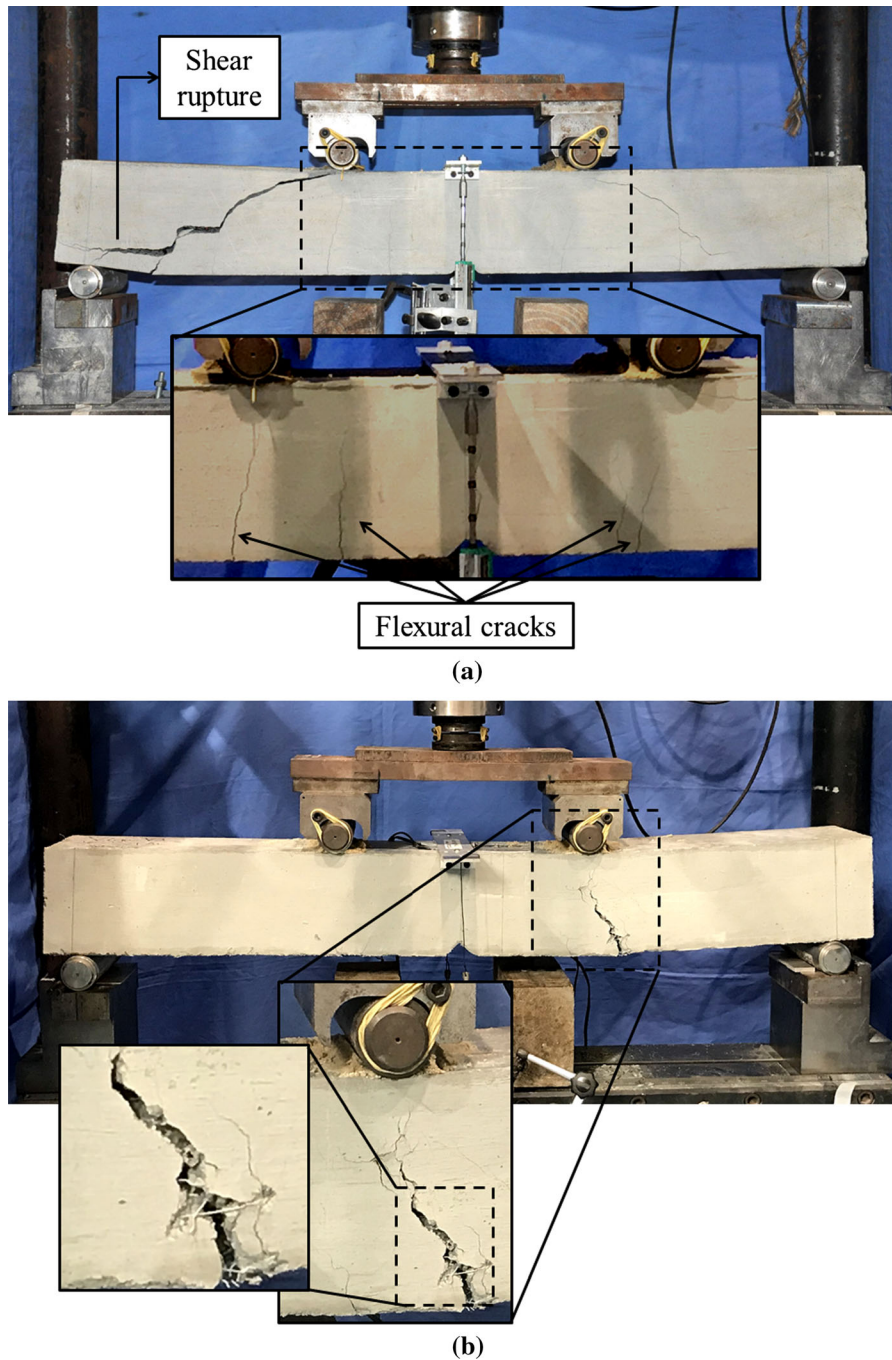
(a)

(b)

Fig. 9 **a** Shear failure (SBR-L0% beam); **b** failure by shear and flexure (SBR-L2% beam)

of concrete obtained for a certain crack opening (Model Code [74] recommends for 2.5 mm) or from direct tensile tests; f_t is the tensile strength of the textile reinforcement; ρ_t is the longitudinal textile reinforcement ratio; and η and λ are coefficients for the parabola-rectangle diagram of the concrete compression zone. It was assumed $\eta = 1$ and $\lambda = 0.8$. The residual tensile strength of concrete was obtained from
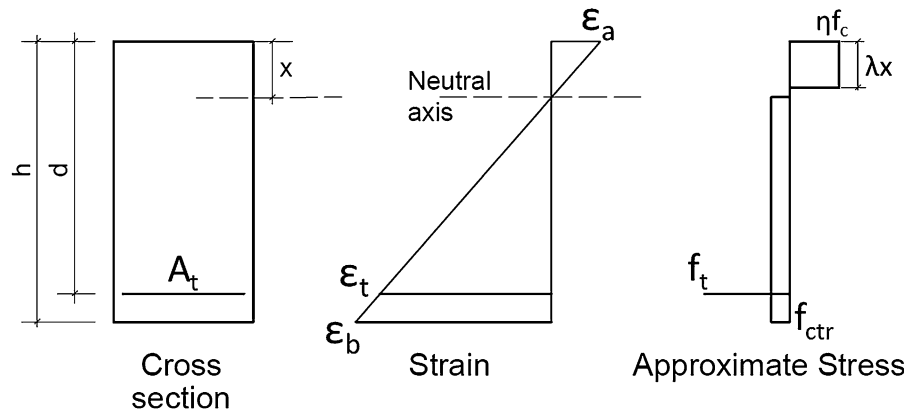
Fig. 10 Beam geometry, strain and approximate stress distribution based on Henager and Doherty's model

Cardoso et al. [75], since the concrete matrix used was the same of this research.

Table 3 shows the results obtained for the theoretical maximum bending moments. The significant difference between the experimental and theoretical results of the SBR-L0% and EPX-L0% beams may have been caused due to their shear failure. Therefore, these beams were not able to reach their maximum bending capacity. The EPX-L2% beam also presented a significant difference between the experimental and Henager and Doherty's model theoretical results, which may also be related to the shear failure of the beam. By the other hand, the difference in experimental and Rilem Report 36 method theoretical results was lower. This may have occurred because this method does not consider the residual tensile strength of concrete. Therefore, the theoretical maximum bending capacity could be under-designed. For the SBR-L2% beam, the difference between the experimental and theoretical results was not so significant, which may be related to the failure by shear and flexure of the beam. However, it should be noted that the difference between the experimental and the Rilem Report 36 method theoretical results could be underestimated since this method does not consider the residual tensile strength of concrete. The SBR-LT2% beam presented flexure failure, thus reaching its maximum bending capacity. The difference of 0.9 between the experimental and Henager and Doherty's model theoretical results indicates that this method seems to be efficient for the prediction of the bending capacity of textile reinforced concrete beams with the addition of short steel fibers. On the other hand, the Rilem Report 36

model does not seem so efficient. In this case, the difference between experimental and theoretical results was 1.39. Once again, this may be related to the fact that this model does not consider the residual tensile strength of concrete.

Additionally, the carbon TRC beams were compared with steel reinforced concrete (RC) beams with three different steel reinforcing bars diameter, 6.3, 8, and 10 mm and reinforcement ratios of 0.28%, 0.44%, and 0.70%, respectively [75]. The mechanical behavior comparison was made even though the failure mode of the carbon TRC and the RC beams was not the same since all RC beams presented flexure failure. The RC beams had the same dimensions as the carbon TRC beams, and the four-point bending test setup was also the same. Figure 11 shows the load–displacement curves for the carbon TRC and RC beams without (Fig. 11a) and with (Fig. 11b) dispersed steel fibers. Without dispersed steel fibers, the carbon TRC beams presented maximum applied load values between the ones obtained for the RC beams with 6.3 and 8 mm steel reinforcing bars. The addition of the dispersed steel fibers enhanced the maximum applied load of the carbon TRC beams to values similar to the ones obtained for the RC beams with 10 mm reinforcing. Furthermore, the SBR-LT2% beam presented the maximum applied load superior to the RC beam with a 10 mm steel reinforcing bar.

The main difference between the bending behavior of the carbon TRC and RC beams is related to their ductility. Unlikely the steel reinforcing bars, the carbon fabrics present a fragile behavior and no yielding characteristics. Therefore, their failure leads
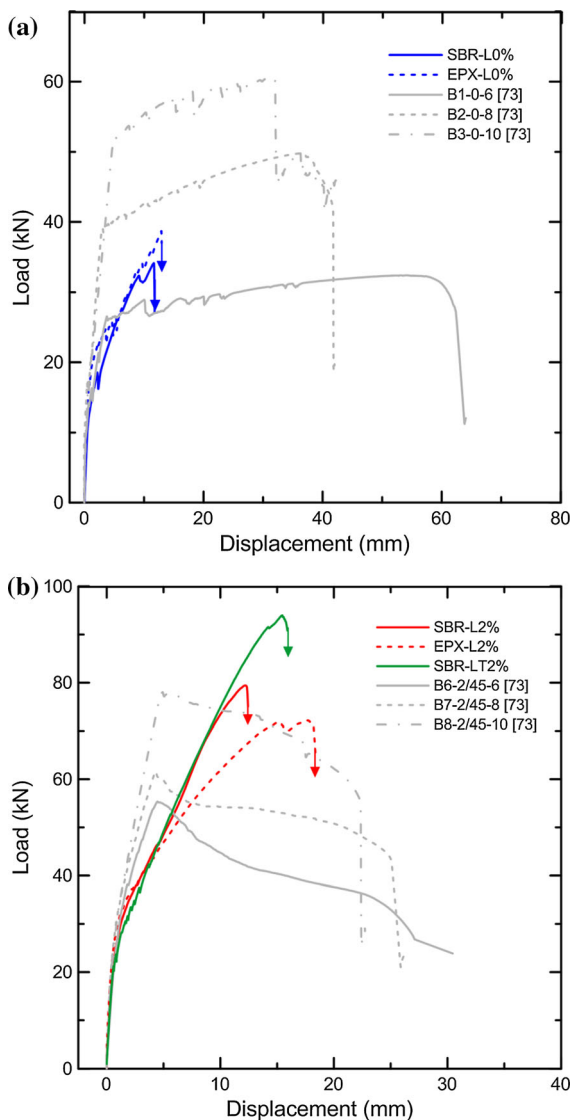
Fig. 11 Load-displacement curves for the carbon TRC and RC beams **a** without, and **b** with dispersed steel fibers

span. In the case of the beams investigated in the present research, the maximum displacement allowed by the NBR 6118:2014 and Fib Model Code would be 4.4 mm. For this displacement level, the load versus displacement curves of the carbon TRC and RC beams is correspondent and the applied load is considerably distant from the maximum values.

The carbon TRC beams present stiffness loss, i.e., the slope of the load versus displacement curve decrease at load levels inferior to the maximum applied load. Consequently, they reach the maximum applied load in displacement levels superior than the RC beams.

4 Conclusions

As expected, all the carbon TRCs submitted to direct tensile loading presented a strain hardening behavior, and the three characteristics distinct zones of TRCs were identified in the tensile stress–strain curves. The tensile performance of the TRC with EPX carbon fabric was superior to the one obtained for the TRC with SBR carbon fabric, suggesting an improved bond between the EPX carbon fabric and the cementitious matrix. This statement is supported by the pull-out test results that demonstrated an increased efficiency of the epoxy resin used as a polymeric coating, providing an enhanced fiber-matrix interaction, when compared to SBR.

The addition of an epoxy resin and sand coating improved the mechanical response under tensile loading of the carbon TRC composites. This improvement was more significant in the TRC with the SBR carbon fabric. Once again the efficiency of the composites under direct tensile loading was confirmed by the pull-out tests.

The TRC with two layers of SBR carbon fabric showed superior tensile strength than the one with only one layer, as expected. However, for the TRC with EPX carbon fabrics, the increase in the number of reinforcement layers did not affect significantly the composite tensile strength. The cross-sectional of the composites with different number of EPX carbon fabric layers was not kept constant, and the addition of one reinforcement layer did not increase significantly the reinforcement volume fraction. Further investigations should be performed in order to analyze if it is more advantageous to increase the number of

to element failure. Hence, the failure of the carbon TRC beams was less ductile than the RC beams, which could limit their use in practical situations. However, the structural elements must satisfy the ultimate limit state (ULS) and the serviceability limit state (SLS), and one of the criteria of the SLS establish limits values for structural elements displacement. According to the Brazilian Code NBR 6118:2014 [58] and the fib Model Code 2010 [74], standards for the design of reinforced concrete elements, a structural element displacement has to be less than l/250, where l is its

reinforcement layers or to add an epoxy resin and sand coating to obtain a better performance.

The carbon TRC beams with dispersed steel fibers presented higher bearing capacity load values when compared to the ones manufactured only with carbon fabrics as reinforcement. This indicates that the dispersed reinforcement was able to support part of the shear stresses. However, in the volume content that they were added, the steel fibers could not avoid completely the shear failure of the beams. The addition of the textile reinforcement in the transversal direction was able to completely prevent a shear failure, allowing a flexure-mode of failure to occur.

The TRC beams without steel fibers presented maximum applied load in the same level of the RC beams with reinforcement ratios of 0.28% and 0.44%. The incorporation of dispersed steel fibers in the carbon TRC beams resulted in maximum applied loads in the same level of the RC beam with 0.70% reinforcement ratio. Additionally, the carbon TRC beam with textile reinforcement in the transversal direction was able to reach a maximum applied load superior to the RC beam with 0.70% reinforcement ratio. The main difference between the carbon TRC beams and the RC beams is regarding their ductility since the carbon fabric does not present yielding characteristics. Nevertheless, this issue would not limit the use of the carbon TRC beams in practical situations, since structural elements must satisfy both limit state values (ULS) and the serviceability limit state (SLS) that restrain the maximum displacement allowed. In these displacement levels, both carbon TRC and RC beams load versus displacement curves are correspondents and the applied load is considerably distant from the maximum values.

Compliance with ethical standards

Conflict of interest　The authors declare that they have no conflict of interest.

References

1. Naaman AE (2010) Textile reinforced cement composites: competitive status and research directions. In: International RILEM conference on materials science (MatSci), pp 3–22

2. Zhu D, Gencoglu M, Mobasher B (2009) Low velocity flexural impact behavior of AR glass fabric reinforced cement composites. Cem Concr Compos 31:379–387. https://doi.org/10.1016/j.cemconcomp.2009.04.011

3. de Silva FA, Butler M, Mechtcherine V et al (2011) Strain rate effect on the tensile behaviour of textile-reinforced concrete under static and dynamic loading. Mater Sci Eng A 528:1727–1734. https://doi.org/10.1016/j.msea.2010.11.014

4. Barhum R, Mechtcherine V (2012) Effect of short, dispersed glass and carbon fibres on the behaviour of textile-reinforced concrete under tensile loading. Eng Fract Mech 92:56–71. https://doi.org/10.1016/j.engfracmech.2012.06.001

5. Du Y, Zhang M, Zhou F, Zhu D (2017) Experimental study on basalt textile reinforced concrete under uniaxial tensile loading. Constr Build Mater 138:88–100. https://doi.org/10.1016/j.conbuildmat.2017.01.083

6. Du Y, Zhang X, Zhou F et al (2018) Flexural behavior of basalt textile-reinforced concrete. Constr Build Mater 183:7–21. https://doi.org/10.1016/j.conbuildmat.2018.06.165

7. Silva F de A, Filho RDT, Filho JAM, Fairbairn EMR (2007) Effect of reinforcement ratio on the mechanical response of compression molded sisal fiber textile reinforced concrete. In: High performance fiber reinforced cement composites (HPFRCC5), pp 175–182

8. de Silva FA, Mobasher B, Filho RDT (2009) Cracking mechanisms in durable sisal fiber reinforced cement composites. Cem Concr Compos 31:721–730. https://doi.org/10.1016/j.cemconcomp.2009.07.004

9. Hakamy A, Shaikh FUA, Low IM (2014) Characteristics of hemp fabric reinforced nanoclay-cement nanocomposites. Cem Concr Compos 50:27–35. https://doi.org/10.1016/j.cemconcomp.2014.03.002

10. Fidelis MEA, de Andrade Silva F, Toledo Filho RD (2014) The influence of fiber treatment on the mechanical behavior of jute textile reinforced concrete. Key Eng Mater 600:469–474. https://doi.org/10.4028/www.scientific.net/KEM.600.469

11. Dvorkin D, Poursaee A, Peled A, Weiss WJ (2013) Influence of bundle coating on the tensile behavior, bonding, cracking and fluid transport of fabric cement-based composites. Cem Concr Compos 42:9–19. https://doi.org/10.1016/j.cemconcomp.2013.05.005

12. Dvorkin D, Peled A (2016) Effect of reinforcement with carbon fabrics impregnated with nanoparticles on the tensile behavior of cement-based composites. Cem Concr Res 85:28–38. https://doi.org/10.1016/j.cemconres.2016.03.008

13. Halvaei M, Latifi M, Jamshidi M (2018) Study of the microstructure and flexural behavior of cementitious composites reinforced by surface modified carbon textiles. Constr Build Mater 158:243–256. https://doi.org/10.1016/j.conbuildmat.2017.10.044

14. Brameshuber W (2006) Report 36: textile reinforced concrete-state-of-the-art report of RILEM TC 201-TRC. Rilem Publications, Paris

15. Brückner A, Ortlepp R, Curbach M (2006) Textile reinforced concrete for strengthening in bending and shear. Mater Struct 39:741–748. https://doi.org/10.1617/s11527-005-9027-2

16. Ambrisi AD, Focacci F (2011) Flexural strengthening of RC beams with cement-based composites. J Compos Constr 15:707–720. https://doi.org/10.1061/(ASCE)CC.1943-5614.0000218

17. Kouris LAS, Triantafillou TC (2018) State-of-the-art on strengthening of masonry structures with textile reinforced mortar (TRM). Constr Build Mater 188:1221–1233. https://doi.org/10.1016/j.conbuildmat.2018.08.039

18. Koutas LN, Tetta Z, Bournas DA, Triantafillou TC (2019) Strengthening of concrete structures with textile reinforced mortars: state-of-the-art review. J Compos Constr. https://doi.org/10.1061/(ASCE)CC.1943-5614.0000882

19. Ombres L (2011) Flexural analysis of reinforced concrete beams strengthened with a cement based high strength composite material. Compos Struct 94:143–155. https://doi.org/10.1016/j.compstruct.2011.07.008

20. Al-Salloum YA, Elsanadadey HM, Alsayed SH, Iqbal RA (2012) Experimental and numerical study for the shear strengthening of reinforced concrete beams using textile-reinforced mortar. J Compos Constr 16:74–90. https://doi.org/10.1061/(ASCE)CC.1943-5614.0000239

21. Schladitz F, Frenzel M, Ehlig D, Curbach M (2012) Bending load capacity of reinforced concrete slabs strengthened with textile reinforced concrete. Eng Struct 40:317–326. https://doi.org/10.1016/j.engstruct.2012.02.029

22. Loreto G, Leardini L, Arboleda D, Nanni A (2013) Performance of RC slab-type elements strengthened with fabric-reinforced cementitious-matrix composites. J Compos Constr 18:A4013003. https://doi.org/10.1061/(ASCE)CC.1943-5614.0000415

23. Babaeidarabad S, De Caso F, Nanni A (2013) URM walls strengthened with fabric-reinforced cementitious matrix subjected to diagonal compression. J Compos Constr 18:04013045. https://doi.org/10.1061/(ASCE)CC.1943-5614.0000441

24. Babaeidarabad S, Loreto G, Nanni A (2014) Flexural strengthening of RC beams with an externally bonded fabric-reinforced cementitious matrix. J Compos Constr 18:04014009-1–04014009-12

25. Azam R, Soudki K (2014) FRCM strengthening of shear-critical RC beams. J Compos Constr 18:04014012. https://doi.org/10.1061/(ASCE)CC.1943-5614.0000464

26. Tetta ZC, Triantafillou TC, Bournas DA (2018) On the design of shear-strengthened RC members through the use of textile reinforced mortar overlays. Compos Part B Eng 147:178–196. https://doi.org/10.1016/j.compositesb.2018.04.008

27. Schumann A, Michler H, Schladitz F, Curbach M (2018) Parking slabs made of carbon reinforced concrete. Struct Concr 19:647–655. https://doi.org/10.1002/suco.201700147

28. May S, Michler H, Schladitz F, Curbach M (2018) Lightweight ceiling system made of carbon reinforced concrete. Struct Concr. https://doi.org/10.1002/suco.201700224

29. May S, Steinbock O, Michler H, Curbach M (2018) Precast slab structures made of carbon reinforced concrete. Structures. https://doi.org/10.1016/j.istruc.2018.11.005

30. Salmon DC, Einea A, Tadros MK, Culp TD (1997) Full scale testing of precast concrete sandwich panels. ACI Struct J 94:239–247

31. Hegger J, Zell M, Horstmann M (2008) Textile reinforced concrete-realization in applications. Symp Tailor Made Concr Struct. https://doi.org/10.1201/9781439828410.ch61

32. Hegger J, Schneider H, Sherif A et al (2004) Exterior cladding panels as an application of textile reinforced concrete. Am Concr Inst 224:55–70

33. Colombo IG, Colombo M, Di Prisco M (2015) Bending behaviour of textile reinforced concrete sandwich beams. Constr Build Mater 95:675–685. https://doi.org/10.1016/j.conbuildmat.2015.07.169

34. Anh Nguyen V, Jesse F, Curbach M (2016) Experiments to establish the loadbearing behaviour of lightweight sandwich beams using textile-reinforced and expanded polystyrene concrete. Struct Concr 17:760–767. https://doi.org/10.1002/suco.201500156

35. Junes A, Si Larbi A (2016) An experimental and theoretical study of sandwich panels with TRC facings: use of metallic connectors and TRC stiffeners. Eng Struct 113:174–185. https://doi.org/10.1016/j.engstruct.2016.01.042

36. Scholzen A, Chudoba R, Hegger J (2015) Thin-walled shell structures made of textile-reinforced concrete: Part I: structural design and construction. Struct Concr 16:106–114. https://doi.org/10.1002/suco.201300071

37. Scholzen A, Chudoba R, Hegger J (2015) Thin-walled shell structures made of textile-reinforced concrete: Part II: experimental characterization, ultimate limit state assessment and numerical simulation. Struct Concr 16:115–124. https://doi.org/10.1002/suco.201400046

38. Sharei E, Scholzen A, Hegger J, Chudoba R (2017) Structural behavior of a lightweight, textile-reinforced concrete barrel vault shell. Compos Struct 171:505–514. https://doi.org/10.1016/j.compstruct.2017.03.069

39. Hegger J, Curbach M, Stark A et al (2018) Innovative design concepts: application of textile reinforced concrete to shell structures. Struct Concr 19:637–646. https://doi.org/10.1002/suco.201700157

40. Poursaee A (2016) Corrosion of steel in concrete structures. Elsevier, Amsterdam

41. Rodriguez J, Ortega LM, Casal J (1997) Load carrying capacity of concrete structures. Constr Build Mater 11:239–248. https://doi.org/10.1016/S0950-0618(97)00043-3

42. Stanish K, Hooton RD, Pantazopoulou SJ (1999) Corrosion effects on bond strength in reinforced concrete. ACI Struct J 96:915–921

43. Almusallam AA (2001) Effect of degree of corrosion on the properties of reinforcing steel bars. Constr Build Mater 15:361–368

44. Ouglova A, Berthaud Y, Foct F et al (2008) The influence of corrosion on bond properties between concrete and reinforcement in concrete structures. Mater Struct Constr 41:969–980. https://doi.org/10.1617/s11527-007-9298-x

45. Chand S (2000) Review: carbon fibers for composites. J Mater Sci 35:1303–1313. https://doi.org/10.1023/A:1004780301489

46. Sauder C, Lamon J, Pailler R (2004) The tensile behavior of carbon fibers at high temperatures up to 2400 °C. Carbon N Y 42:715–725. https://doi.org/10.1016/j.carbon.2003.11.020

47. Bentur A, Mindess S (2006) Fiber reinforced cementitious composites. CRC Press, Boca Raton

48. Arboleda D, Babaeidarabad S, Nanni A (2014) Durability of fabric reinforced cementitious matrix (FRCM) composites. In: 7th International conference of frp composites in civil engineering. International Institute for FRP in Construction, pp 1–6

49. Schuetze E, Lorenz E, Curbach M (2015) Static and dynamic fatigue strength of textile reinforced concrete. In: IABSE symposium report

50. Peled A, Mechtcherine V, Nicke D, Hempel S (2015) Modifying carbon roving-cement matrix bond by inorganic coating. In: Reinhardt HW, Parra-Montesino GJ, Garrencht H (eds) High performance fiber reinforced cement composites (HPFRCC7). RILEM, Struttgart, Germany, pp 61–67

51. Schneider K, Michel A, Liebscher M et al (2019) Mineral-impregnated carbon fibre reinforcement for high temperature resistance of thin-walled concrete structures. Cem Concr Compos 97:68–77. https://doi.org/10.1016/j.cemconcomp.2018.12.006

52. Triantafillou TC (2016) Textile fibre composites in civil engineering. Woodhead Publishing, Sawston

53. Donnini J, Corinaldesi V, Nanni A (2016) Mechanical properties of FRCM using carbon fabrics with different coating treatments. Compos Part B Eng 88:220–228. https://doi.org/10.1016/j.compositesb.2015.11.012

54. Xu S, Krüger M, Reinhardt H-W, Ožbolt J (2004) Bond Characteristics of carbon, alkali resistant glass, and aramid textiles in mortar. J Mater Civil Eng 16:356–364. https://doi.org/10.1061/(ASCE)0899-1561(2004)16:4(356)

55. Brazilian Standard NBR 11578 (1991) Cimento Portland composto. Associação Brasileira de Normas Técnicas (ABNT)

56. Brazilian Standard NBR 5733 (1991) Cimento Portland de alta resistência inicial. Associação Brasileira de Normas Técnicas (ABNT)

57. Silva RM de C, Silva F de A (2018) Mechanical and bond behavior of carbon textile reinforced concretes under tensile loading. In: Silva F de A, D'Almeida JRM, Cardoso DCT, Souza LMS (eds) 4th Brazilian conference on composite materials. Rio de Janeiro, pp 289–297

58. Brazilian Standard NBR 6118 (2014) Projeto de estruturas de concreto-Procedimento

59. Bähr LT d'Azevedo L (2016) Mechanical behavior and numerical modeling of textile reinforced concrete. Pontifícia Universidade Católica do Rio de Janeiro (PUC-Rio)

60. Yin S, Wang B, Wang F, Xu S (2017) Bond investigation of hybrid textile with self-compacting fine-grain concrete. J Ind Text 46:1616–1632. https://doi.org/10.1177/1528083716629137

61. Donnini J, De Caso y Basalo F, Corinaldesi V et al (2017) Fabric-reinforced cementitious matrix behavior at high-temperature: experimental and numerical results. Compos Part B Eng 108:108–121. https://doi.org/10.1016/j.compositesb.2016.10.004

62. Holz K, Schütze E, Garibaldi P, Curbach M (2018) Determination of Material Properties of TRC Under Cyclic Loads. Spec Publ 324:1.1-1.16

63. Xu S, Li H (2007) Bond properties and experimental methods of textile reinforced concrete. J Wuhan Univ Technol Mater Sci Ed 22:529–532. https://doi.org/10.1007/s11595-006-3529-9

64. Hinzen M, Brameshuber W (2007) Influence of short fibres on strength, ductility and crack development of textile reinforced concrete. In: Proceedings of the fifth international RILEM workshop on high performance fiber reinforced cement composites (HPFRCC5). RILEM Proceedings PRO, pp 105–112

65. Mansur MA, Ong KCG, Paramasivam P (1986) Shear strength of fibrous concrete beams without stirrups. J Struct Eng 112:2066–2079

66. Lim DH, Oh BH (1999) Experimental and theoretical investigation on the shear of steel fibre reinforced concrete beams. Eng Struct 21:937–944. https://doi.org/10.1016/S0141-0296(98)00049-2

67. Cucchiara C, La Mendola L, Papia M (2004) Effectiveness of stirrups and steel fibres as shear reinforcement. Cem Concr Compos 26:777–786. https://doi.org/10.1016/j.cemconcomp.2003.07.001

68. Dinh H, Parra-Montesinos GJ, Wight JK (2011) Shear strength model for steel fiber reinforced concrete beams without stirrup reinforcement. J Struct Eng 137:1039–1051. https://doi.org/10.1061/(ASCE)ST.1943-541X.0000362

69. Hegger J, Kulas C, Schneider HN, et al (2010) TRC pedestrian bridge-design, load-bearing behavior and production processes of a slender and light-weight construction. In: International RILEM conference on material science. RILEM Publications SARL, pp 353–364

70. Jelić I, Pavlović MN, Kotsovos MD (1999) A study of dowel action in reinforced concrete beams. Mag Concr Res 51:131–141. https://doi.org/10.1680/macr.1999.51.2.131

71. Grace NF, Soliman AK, Abdel-Sayed G, Saleh KR (1998) Behavior and ductility of simple and continuous FRP reinforced beams. J Compos Constr 2:186–194. https://doi.org/10.1061/(ASCE)1090-0268(1998)2:4(186)

72. El-Ariss B (2007) Behavior of beams with dowel action. Eng Struct 29:899–903. https://doi.org/10.1016/j.engstruct.2006.07.008

73. Henager CH, Doherty TJ (1976) Analysis of reinforced fibrous concrete beams. J Struct Div 102:177

74. International Federation for Structural Concrete (2012) Fib model code: bulletin 66

75. Cardoso DCT, Pereira GBS, Silva FA et al (2019) Influence of steel fibers on the flexural behavior of RC beams with low reinforcing ratios: analytical and experimental investigation. Compos Struct 222:110926. https://doi.org/10.1016/j.compstruct.2019.110926